Curvilinear-Coordinate-Based Object and Situation Assessment for Highly Automated Vehicles

Junsoo Kim, *Student Member, IEEE*, Kichun Jo, *Member, IEEE*, Wontaek Lim, *Student Member, IEEE*, Minchul Lee, *Student Member, IEEE*, and Myoungho Sunwoo, *Member, IEEE*

Abstract—This paper presents a novel curvilinear-coordinate-based approach to improve object and situation assessment performance for highly automated vehicles under various curved road conditions. The approach integrates object information from radars and lane information from a camera with three steps: track-to-track fusion, curvilinear coordinate conversion, and lane assessment. The track-to-track fusion is achieved through a nearest neighbor filter that updates the target state estimation and covariance with the nearest neighbor measurement, and a cross-covariance method that merges the duplicate tracks using error covariance. In order to determine in which lane the fused tracks are located accurately and reliably, the curvilinear coordinate conversion process is performed. The curvilinear coordinates are generated in the form of a cubic Hermite spline lane model from the lane information of the camera. Based on the converted track information and the lane model in the curvilinear coordinates, the probability distribution of the threat levels in each lane is determined though a probabilistic lane association and threat assessment. The developed algorithm is verified and evaluated through experiments using a real-time embedded system. The results show that the proposed curvilinear-coordinate-based approach provides excellent performance of object and situation assessment, in respect of accuracy and computational efficiency, in real-time operation.

Index Terms—Curvilinear coordinates, data fusion, intelligent vehicle, object detection and tracking, situation assessment.

I. INTRODUCTION

IN recent years, many studies for intelligent transportation systems (ITS) have been conducted in the areas of vehicle safety, passenger comfort, and system sustainability. Various types of advanced driver-assistance systems (ADAS), such as adaptive cruise control (ACC), lane keeping assistance (LKA), blind spot detection (BSD), and parking assistance,

The authors are with the Automotive Control and Electronics Laboratory, Department of Automotive Engineering, Hanyang University, Seoul 133-791, Korea (e-mail: junskys@gmail.com; jokihaha@hanyang.ac.kr; lwt1849@gmail.com; minchulmando@gmail.com; msunwoo@hanyang.ac.kr).

have been successfully developed for passenger vehicles. To further enhance safety and convenience, considerable research activities have focused on highly automated driving, such as the Safe Road Trains for the Environment (SARTRE) Project [1], [2], the Highly Automated Vehicles for Intelligent Transport (HAVEit) Project [3], [4], the Defense Advanced Research Projects Agency Urban Challenge [5], [6], and the Grand Cooperative Driving Challenge [7], [8]. Through these research activities, the technical feasibility of highly automated vehicles has been demonstrated. However, significant challenges still remain, in terms of reliability, cost, and legislation [9]. For example, reliable perception and decision of the vehicle's environment can be derived from high-quality sensor data, but that can cause cost problems. Therefore, the gap between strict reliability constraints and limited sensor data quality is one of the most challenging issues.

In order to improve perception and decision performance, multisensor-based data fusion techniques have received a great deal of attention in automotive applications. The data fusion techniques combine data from multiple sensors and related information to achieve more specific inferences than can be achieved using a stand-alone sensor [10]. Therefore, multisensor-based data fusion techniques are widely used in many applications.

There are two major functions for multisensor-based data fusion: an *object assessment* and a *situation assessment* [11], [12]. According to the revised data fusion model proposed by the U.S. Joint Directors of Laboratories (JDL) Data Fusion Group [11], [12], the object assessment is defined as "estimation and prediction of entity states on the basis of inferences from observations." Since the observations from sensors may be imprecise and uncertain, the object assessment focuses on the estimates of the object's state for reduction of the uncertainty through filtering algorithms (e.g., Kalman and particle filter) with probabilistic models about system dynamics and sensor characteristics [13]. The situation assessment is related to the interpretation of a driving situation from the results of the object assessment. Definition of the situation assessment in the JDL data fusion model is "estimation and prediction of entity states on the basis of inferred relations among entities." Thus, the situation assessment should evaluate the complicated relationships among the detected entities, in order to determine appropriate system reactions under real worlds [13].

When these two functions are applied in real road driving, the more complicated practical problems are incurred by road environments [14]. Since the vehicle motion is not linear for curved roads, the assessments can be regarded as geometrically
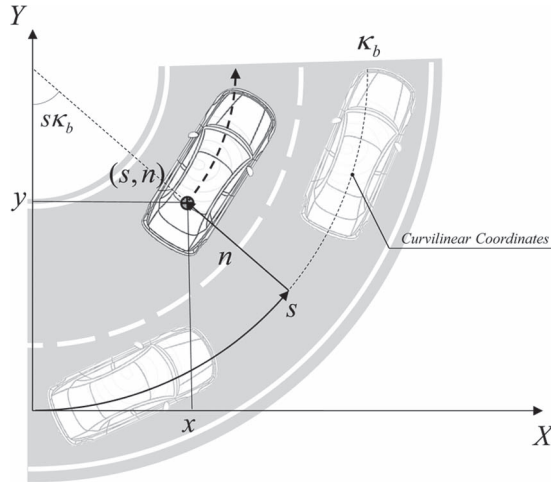
Fig. 1. Example of vehicle trajectory representation on the Cartesian coordinates and the curvilinear coordinates.

complex problems in Cartesian coordinates, as shown in Fig. 1. In addition, the numerical computation to solve the geometric problems in the Cartesian coordinates should be reliable for real-time implementation. Thus, the geometry of physical problems may make non-Cartesian coordinates (e.g., the curvilinear coordinates [15]–[17]) more suitable as a basis for analysis [18].

In this paper, we propose a practical object and situation assessment method based on decentralized fusion and a probabilistic assessment technique for highly automated vehicles using the curvilinear coordinates. This paper was motivated by [13] and [19], which introduced a well-established unified Bayesian approach for object and situation assessment. Through this approach, a unified method of representing uncertainties can be achieved from the object assessment to the situation assessment. However, since the unified Bayesian approach used a circle lane model in the lane association that determines in which lane an object exists, an accuracy problem might occur in the situation assessment. The reason for the problem is that the circular lane model has high approximation errors in the representation of complex road shapes. In order to complement previous research, this paper applies the curvilinear coordinates [15] to object and situation assessment.

The proposed method in this paper consists of three parts: *track-to-track fusion*, *curvilinear coordinate conversion*, and *lane assessment*. The track-to-track fusion part is composed of a nearest neighbor filter (NNF) and a cross-covariance method (CCM)-based fusion algorithm for merging the object information from multiple radars. In order to achieve not only a simple analytic formula but also reliable numerical computations for the lane association, the curvilinear coordinate conversion converts Cartesian coordinates into curvilinear coordinates, using the road geometry information. The road geometry information is derived from lane data with a front camera. Finally, the lane assessment evaluates the curvilinear-coordinate-based lane status through the probabilistic lane association and threat assessment.

The rest of this paper is organized as follows. Section II introduces related research work. In Section III, the problems for the object and situation assessment are formulated, and the

overall system architecture is discussed. From Section IV to Section VI, the NNF- and CCM-based track-to-track fusion, the curvilinear coordinate conversion, and the curvilinear-coordinate-based situation assessment are explained, respectively. The experimental results that were obtained from the highway tests are presented in Section VII. Finally, the conclusion is provided in Section VIII.

II. RELATED RESEARCH

In order to categorize data-fusion-related functions in the various data fusion applications, a data fusion model was proposed by the U.S. JDL Data Fusion Group [11], [12]. The JDL data fusion model defines five data-fusion functional levels: *signal/feature assessment* (Level 0), *object assessment* (Level 1), *situation assessment* (Level 2), *impact assessment* (Level 3), and *process assessment* (Level 4). Signal/feature assessment encompasses various uses of multiple measurements in signal and feature processing, such as feature extraction from images, noise filtering in analog signals, and parameter estimation in motor control. The notion of object assessment is conceived as the most highly developed applications of data fusion: detection, identification, location, and tracking of individual objects. Situation assessment involves inferring relationships from the estimated states of one object in a situation to another and from the estimated attributes and relationships of objects to situations. Impact assessment is defined as the estimation of effects on situations of planned or predicted actions by participants. Finally, the process assessment combines information to estimate a system's measure of performance based on a desired set of system states and responses. In this paper, we focus on object and situation assessment (Levels 1 and 2) algorithms that provide reliable driver assistance capability to a highly automated vehicle under various environmental conditions.

A. Object Assessment

The object assessment can generally be categorized as *centralized fusion* and *decentralized fusion* [20], [21]. In centralized fusion, the measurements from the sensors are fused to obtain a weighted or combined measurement in a central site, and a single filtering algorithm (e.g., Kalman filter, particle filter, Bayes estimators, and so on) is used to obtain a final optimal state estimate based on this fused observation. In the decentralized fusion, multiple sensors have their own tracking algorithm to determine a track state estimation. The estimated results of each sensor are transferred to a central computing unit with the covariance of the track estimates. Finally, the central unit performs track association and track management for track-to-track fusion.

Generally, the centralized fusion usually provides better overall tracking performance due to the centralized full-information estimation. However, it requires a lot of computational resources, and it is hard to guarantee fault tolerance [22], [23]. Otherwise, decentralized fusion is suboptimal but more efficient [21]. In addition, vehicle sensors, such as radars and cameras, are produced by various automotive suppliers. The sensors usually provide processed data or a tracked object list from raw data. Even if the raw sensor data can be accessed,

hardware-specific knowledge should be fully understood, in order to take full advantage of raw sensor data. Therefore, decentralized fusion is preferred in object assessment [24].

In decentralized fusion, there are well-established approaches to fuse state vectors: cross-covariance [25], covariance intersection [26], covariance union [27], and information matrix [28]. These can be used to consider common process noises, asynchronous filtering effect, and temporal sensor correlation, to improve efficiency and accuracy, because the approaches are based on the covariance of track estimates [24]. However, since the previous approaches do not consider the environmental constraints associated with road geometries in urban roads or highways, there are some limitations to object assessment in automotive applications: false positives due to highway guardrails, missing track on curved roads, and so on.

B. Situation Assessment

In order to derive further descriptions of a vehicle's environment, the importance of situation assessment algorithms increases in automotive applications [13]. The main challenge of the situation assessment is on inferring the spatial and temporal relationships between the ego vehicle and the perceived entities. For recognizing and classifying situations from the inferring results, the research approaches about situation assessment algorithms are divided into two categories: the *deterministic approach* and the *probabilistic approach*. The deterministic approach refers to simple methods that infer situation states from the current states of all objects, and use these to compute various threat measures: time to collision (TTC), time to brake, time to steer [29], predicted minimum distance, and predicted time to minimum distance [30]. Deterministic-approach-based algorithms have less computational complexity; hence, they are effectively used in various collision mitigation systems [29]–[31]. However, deterministic-approach-based algorithms employ rule-based expert systems, which do not explicitly model uncertainties in their input data. Therefore, for handling uncertainties, situation assessment algorithms are currently shifting from the deterministic approach toward the probabilistic approach [32].

In order to account for the uncertainties, the probabilistic approach uses a probabilistic description of the vehicle's environment, including probabilistic models of the system dynamics and the sensor properties [13]. For the implementation of the probabilistic approach, various methods have been applied, such as Bayesian networks [33] and the Markov process [34]. These methods can handle incomplete and imprecise data, and data with uncertain properties, but there are interface limitations between object and situation assessments. For example, an object assessment module provides a probability density function (PDF) for each track, but conventional methods require a translation of the uncertainties from one domain to another. In order to overcome these limitations, a well-established unified Bayesian approach for object and situation assessment was recently introduced in [13] and [19]. The interface of the proposed unified Bayesian approach can be also applied in the opposite direction. That is, knowledge about the current traffic situation can be exploited to improve object assessment results.
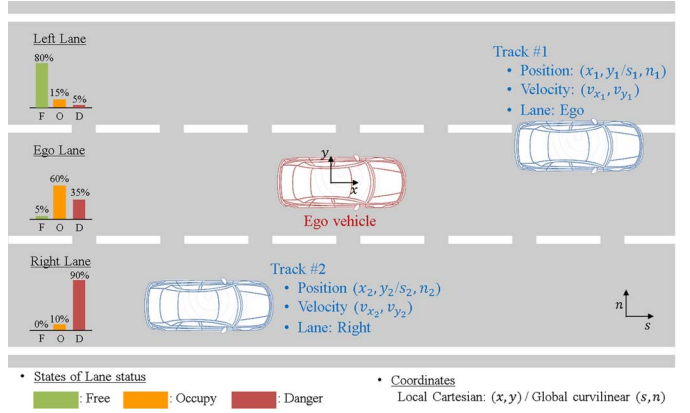

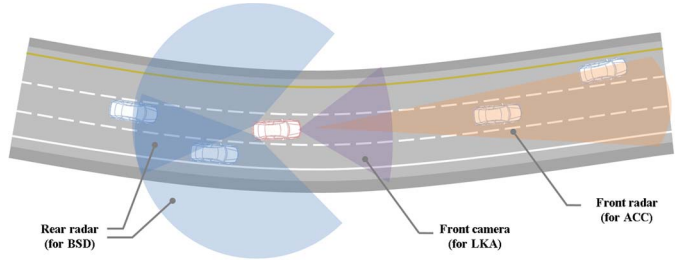Fig. 2. Example of object and situation assessment.

Fig. 3. Sensor configuration of the test vehicle.

However, since the proposed unified Bayesian approach uses a circle lane model for a stable basis in the situation assessment, an accuracy problem can occur in the distance calculation of the lane association. A cubic polynomial lane model can improve distance accuracy compared to the circle model case. However, a convergence speed problem in the numerical computations can occur because derivative-function-based numerical analysis techniques (e.g., Newton's method) are sensitive to rapid changes in the curvature of curved roads. Therefore, an accurate and reliable lane representation method is required, in order to improve the situation assessment under various road geometries.

III. SYSTEM OVERVIEW

A. Problem Formulation

For safe driving, the perception system of ADAS or highly automated vehicles detects various objects such as lanes, vehicles, motorcycles, and pedestrians. The states of lanes and vehicles are particularly important information in highway or urban road driving. The object and situation assessment system can perceive its environment and assess the traffic situation based on this information. Fig. 2 shows an example of an object and situation assessment representing a situation in highway or urban driving. In Fig. 2, the road is composed of three lanes, and two other vehicles move in front of and to the right of the ego vehicle, respectively. In this situation, the ego vehicle should detect the lane shape and track the positions and velocities of other vehicles to evaluate each lane status. To detect the lane and vehicles, a camera and three radars can be used in conventional ADAS applications, as shown in Fig. 3.
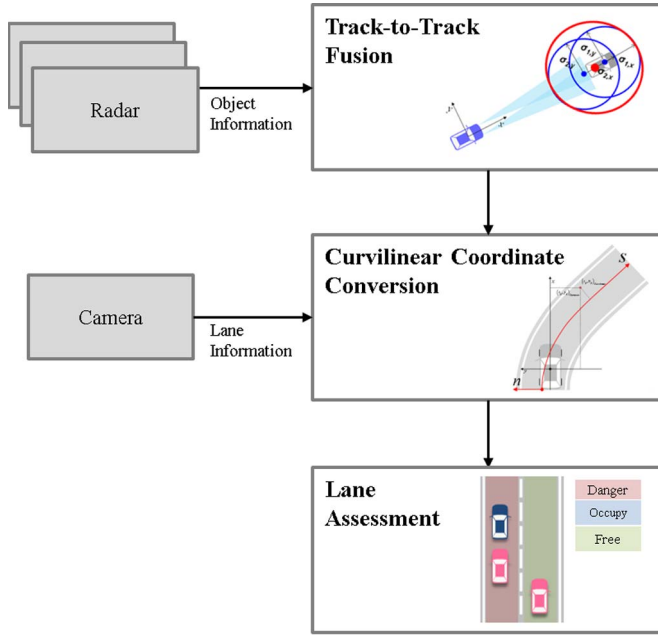
Fig. 4.   System architecture.

The camera for LKA is used to provide a lane model and parameters, which are derived from a processed image source [35], [36]. A long-range radar is located in the front bumper and is used for ACC [37]. Two other middle-range radars are installed in the rear bumper and are used for BSD [38]. Each radar sensor provides state information for the tracked object, such as the position and velocity. Based on the lane and object information, the ego vehicle should evaluate the lane position of each object and assess the status of each lane for driver assistance or autonomous driving.

B. System Architecture

The system architecture to perform object and situation assessment is divided into three steps, as shown in Fig. 4: track-to-track fusion, curvilinear coordinate conversion, and lane assessment. First, the radar sensors give the object information around the ego vehicles. Since there is an overlapped area between the rear radar sensors, as shown in Fig. 3, there may be duplicated data for the same object. In addition, the data from different radar sensors are not synchronized to a common clock; hence, there might not be correlation information from each sensor's filtering algorithm. In order to overcome these problems, the NNF is applied as preprocessing for track generation, and the CCM is used for track fusion in the track-to-track fusion step. The NNF propagates the state and covariance of the tracks using radar object information, and the CCM fuses the tracks for the same object. In the curvilinear coordinate conversion step, an arc-length parameterized curve model is generated from the lane data with a front camera. Based on the lane model, a curvilinear coordinate is formulated, and the coordinate of the tracked object information is converted from a Cartesian to a curvilinear coordinate. In the final step, the curvilinear-coordinate-based object information is used for lane assessment. The probability of the lane association is derived
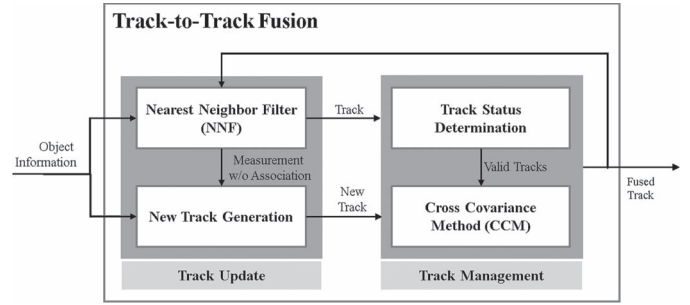

Fig. 5.   NNF- and CCM-based track-to-track fusion.

for each track, and the probability of a threat state is also evaluated using a TTC index. Finally, the probability of lane status, which is related to lane safety, is calculated from the results of lane association and threat assessment.

IV. TRACK-TO-TRACK FUSION

The object data that are received from the radar sensors are composed of position and velocity information. In general, data from different sensors are not synchronized to a common clock and do not provide correlation information from each sensor's filtering algorithm. In order to overcome these difficulties and to improve the object assessment performance, NNF- and CCM-based track-to-track fusion are applied, as shown in Fig. 5. The proposed method is composed of two steps: track update and track fusion. In the track update, the object data from the radar sensors are used as measurement inputs. The NNF updates the states and covariance of track by using the nearest object information within a validation gate. If there is no associated existing track, the object information generates a new track. Based on the track state and covariance, the CCM fuses tracks for the same object and manages the track status.

A. Track Update

1) Mathematical Model for Object Tracking:

a) Prediction Model: In order to generate the states and covariance of the track from the sensor measurements, the NNF is based on the Kalman filter. Since multiple tracks should be managed in real time, we used a simple constant velocity model for the Kalman filter, as

$$X_{k+1} = F_k X_k + G_k w_k$$
$$= \begin{bmatrix} I & T_s I \\ 0 & I \end{bmatrix} X_k + \begin{bmatrix} T_s^2/2I \\ T_s I \end{bmatrix} w_k \qquad (1)$$
$$z_k = H_k X_k + v_k$$
$$= X_k + v_k \qquad (2)$$

where $X = [x\ y\ v_x\ v_y]^T$, T_s is the sampling time, z is the measurement, and w and v are independent zero-mean Gaussian noise variables for the process and measurement with covariance R_w and R_v, respectively. The state X consists of the position and velocity in the vehicle local coordinates: $x, y, v_x,$ and v_y, respectively.
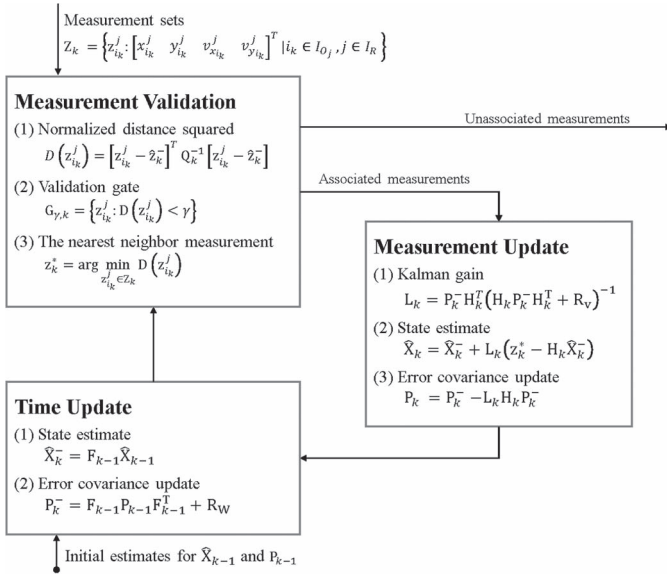
Fig. 6. Operation of an NNF.

b) Measurement Model: From the given radar sensor data, a set of measurements Z_k for object tracking is composed as

$$Z_k = \left\{ z_{0_k}^0 \quad z_{1_k}^0 \quad \cdots \quad z_{i_k}^j \quad \cdots \quad z_{n_k}^m \right\}$$

$$= \left\{ z_{i_k}^j : \left[x_{i_k}^j \quad y_{i_k}^j \quad v_{x_{i_k}}^j \quad v_{y_{i_k}}^j \right]^T | i_k \in I_{O_j}, \; j \in I_R \right\} \quad (3)$$

where I_R is a set of indices of radar sensors $(j = 0, 1, \ldots, m)$, I_{o_j} is a set of indices of the object data for the jth radar sensor $(i = 0, 1, \ldots, n_k)$ at time k, and x_i^j, y_i^j, $v_{x_i}^j$, and $v_{y_i}^j$ are the x and y position and velocity, respectively, of the ith object for the jth radar sensor.

2) NNF: We regarded the estimation of the position and velocity of objects as a problem of tracking multiple targets with multiple measurements. To solve this problem, an NNF was applied [39], [40]. Since the tracks from the radars are sufficiently separated between different targets, the NNF is sufficient for this tracking problem. The NNF assumes, at any time, that the nearest neighbor measurement is target oriented, and a Kalman filter is used to update the target state estimation and covariance with the nearest neighbor measurement. Let z_k^* be the nearest neighbor measurement at time k, which is defined by

$$z_k^* = \arg \min_{z_{i_k}^j \in Z_k} D\left(z_{i_k}^j \right) \quad (4)$$

where the Mahalanobis distance squared $D(z_{i_k}^j)$ is defined as

$$D\left(z_{i_k}^j \right) = \left[z_{i_k}^j - \hat{z}_k^- \right]^T Q_k^{-1} \left[z_{i_k}^j - \hat{z}_k^- \right] \quad (5)$$

where $\hat{z}_k^-$ is the predicted measurement and $Q_k = H_k P_k^- H_k^T + R_v$ is the measurement residual covariance. Based on the nearest neighbor measurement, the NNF is operated as shown in Fig. 6.

a) Process Update: At first, the values of the initial state and error covariance are determined. Then, *a priori* state and error covariance are estimated using the prediction model, as

$$\widehat{X}_k^- = F_{k-1} \widehat{X}_{k-1} \quad (6)$$

$$P_k^- = F_{k-1} P_{k-1} F_{k-1}^T + R_W. \quad (7)$$

b) Measurement Validation: The measurements from the radar sensors are evaluated to determine whether they originated from the target, by using the Mahalanobis distance squared $D(z_{i_k}^j)$ and a validation gate. The validation gate is such a region in the measurement space that only measurements falling inside this region can be associated with the target of interest. The ellipsoidal validation gate $G_{\gamma k}$ is defined as

$$G_{\gamma,k} = \left\{ z_{i_k}^j : D\left(z_{i_k}^j \right) < \gamma \right\} \quad (8)$$

in which $g = \sqrt{\gamma}$ is called the gate size. The nearest neighbor measurement within the validation gate is used for the measurement update of an associated target, and the others are used for other targets or new track generation.

c) Measurement Update: In the measurement update, the NNF updates the Kalman gain L_k by using the measurement matrix H_k, the error covariance P_k, and the measurement residual covariance Q_k, as

$$L_k = P_k^- H_k^T Q_k^{-1}$$
$$= P_k^- H_k^T \left(H_k P_k^- H_k^T + R_v \right)^{-1}. \quad (9)$$

Based on the Kalman gain L_k and the nearest neighbor measurement z_k^*, the posteriori state $\hat{s}_k$ and covariance P_k are derived as

$$\widehat{X}_k = \begin{cases} \widehat{X}_k^- + L_k \left(z_k^* - H_k \widehat{X}_k^- \right), & \text{if } z_k^* \text{ exist} \\ \widehat{X}_k^-, & \text{otherwise} \end{cases} \quad (10)$$

$$P_k = \begin{cases} P_k^- - L_k H_k P_k^-, & \text{if } z_k^* \text{ exist} \\ P_k^-, & \text{otherwise.} \end{cases} \quad (11)$$

3) New Track Generation: If a measurement is not associated with existing tracks, a new track is generated as

$$\widehat{X}_{k,\text{new}} = z_{k,\text{un}} \quad (12)$$

$$P_{k,\text{new}} = R_v \quad (13)$$

where $z_{k,\text{un}}$ is a measurement without an association, and $\hat{s}_{k,\text{new}}$ and $P_{k,\text{new}}$ are the initial state and error covariance, respectively, of a new track.

B. Track Management

Since computational resources are limited and multiple targets should be simultaneously tracked in real time, the track management system is important. To effectively manage the tracks, the proposed algorithm is composed of rule-based track status determination and CCM-based track fusion.
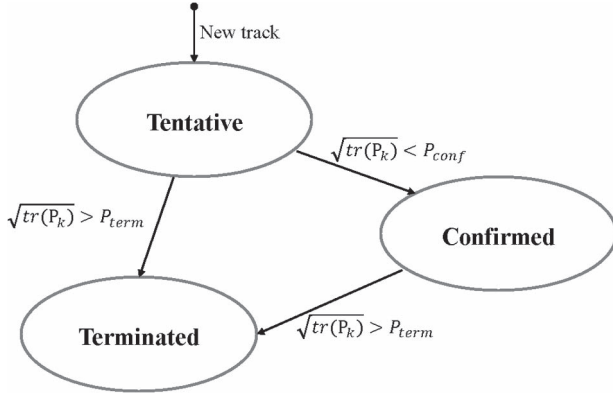
Fig. 7. Track status determination.

Fig. 8. Comparison between Cartesian coordinates and curvilinear coordinates.

1) Rule-Based Track Status Determination: To determine the maintenance or termination of tracks, the quality of the track is evaluated by using the error covariance P_k, as shown in Fig. 7. At first, a newly generated track is categorized as a *tentative track*, which is estimated by using radar data, but is not confirmed as a moving object. As the size of the error covariance is reduced by the measurement update process in the NNF, the track status can be changed to a *confirmed track*. Since confirmed tracks can be regarded as moving vehicles, they are used for the situation assessment. Otherwise, if there are no valid measurements for the track update and the size of the error covariance is increased over the threshold P_{term}, the track status is converted into a *terminated track*, which is no longer estimated.

2) CCM-Based Track Fusion: In order to merge duplicate tracks for the same object, the error covariance of each track is used. If two tracks with tentative or confirmed status are close to each other, the following fusion process is applied:

$$\widehat{X}_{k,3} = \widehat{X}_{k,1} + \chi(\widehat{X}_{k,2} - \widehat{X}_{k,1}) \tag{14}$$

$$P_{k,3} = P_{k,1} - (P_{k,1} - P_{k,1/2})U_{k,1/2}^{-1}(P_{k,1} - P_{k,1/2})^T \tag{15}$$

where

$$\chi = (P_{k,1} - P_{k,1/2})U_{k,1/2}^{-1} \tag{16}$$

$$U_{k,1/2} = P_{k,1} + P_{k,2} - P_{k,1/2} - P_{k,1/2}^T. \tag{17}$$

The cross-covariance matrix $P_{k,1/2}$ is updated using a recursive relationship

$$P_{k,1/2} = \alpha_{k,1}\beta_{k-1}\alpha_{k,2}^T \tag{18}$$

where

$$\alpha_{k,1} = I - L_{k,1}H_{k,1} \tag{19}$$

$$\alpha_{k,2} = I - L_{k,2}H_{k,2} \tag{20}$$

$$\beta_{k-1} = F_{k,1}P_{k-1,1/2}F_{k,2}^T + Q_{k-1}. \tag{21}$$

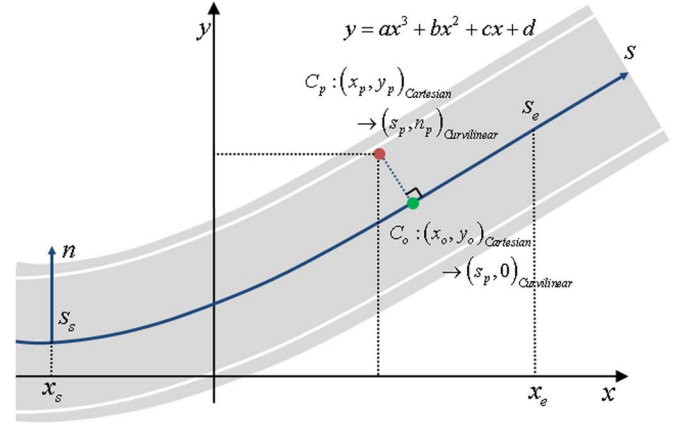Finally, the fused tracks are recursively maintained through the NNF and will be used for situation assessment.

V. Curvilinear Coordinate Conversion

Most radar sensor data are represented in the local Cartesian coordinates. Based on the relative position and velocity information in Cartesian coordinates, most situation assessment algorithms determine the risk of collision under the linear motion assumption. However, it might be misleading in situations where the roads are curved and the assumption does not hold [14]. Therefore, road geometries from the lane information should be considered for accurate situation assessment. However, the relative position and velocity information is not orthogonal to the lane information in Cartesian coordinates; hence, the lane association, which determines the position in the lane, is regarded as a geometrically complex problem. In order to solve the problem, a curvilinear coordinate conversion was applied [15]. In curvilinear coordinates, the problem can be simply solved by the separation of related variables: the lateral (n) and longitudinal (s) directions along a lane, as shown in Fig. 8. In addition, a divergent problem in numerical computations that might occur due to a rapid change in the curvature of the Cartesian coordinates can also be prevented. The curvilinear coordinate conversion process is composed of two steps: the cubic Hermite spline (CHS) lane model generation and the coordinate conversion.

A. CHS Lane Model

Typically, automotive camera sensors provide lane information in a three-order polynomial lane model, as shown in Fig. 8. In order to not only obtain a smooth continuous basis from the lane model but also extrapolate it stably, the CHS is applied to the curvilinear lane model. In order to convert to the CHS, an arc length is first found by numerical integration, as

$$s_s = 0 \tag{22}$$

$$s_e = \int_{x_s}^{x_e} \sqrt{1 + (3ax^2 + 2bx + c)^2}\, dx. \tag{23}$$

Based on the arc length, the CHS is defined as

$$\begin{aligned} C(s) &= [x(s) \quad y(s)]^T \\ &= \vec{a}s^3 + \vec{b}s^2 + \vec{c}s + \vec{d}. \end{aligned} \tag{24}$$

The parameter vectors $(\vec{a}, \vec{b}, \vec{c}, \vec{d})$ can be determined by the boundary conditions, as

$$\vec{a} = \frac{2}{s_e^3} P_s - \frac{2}{s_e^3} P_e + \frac{1}{s_e^2} P_s' + \frac{1}{s_e^2} P_e' \tag{25}$$

$$\vec{b} = -\frac{3}{s_e^2} P_s + \frac{3}{s_e^2} P_e - \frac{2}{s_e} P_s' - \frac{1}{s_e} P_e' \tag{26}$$

$$\vec{c} = P_s' \tag{27}$$

$$\vec{d} = P_s \tag{28}$$

where

$$P_s = C(s_s) = \begin{bmatrix} x_s \\ ax_s^3 + bx_s^2 + cx_s + d \end{bmatrix} \tag{29}$$

$$P_e = C(s_e) = \begin{bmatrix} x_e \\ ax_e^3 + bx_e^2 + cx_e + d \end{bmatrix} \tag{30}$$

$$
\begin{aligned}
P_s' &= C'(s_s) \\
&= \begin{bmatrix} 1/\sqrt{1 + (3ax_s^2 + 2bx_s + c)^2} \\ (3ax_s^2 + 2bx_s + c) / \sqrt{1 + (3ax_s^2 + 2bx_s + c)^2} \end{bmatrix}
\end{aligned}
\tag{31}
$$

$$
\begin{aligned}
P_e' &= C'(s_e) \\
&= \begin{bmatrix} 1/\sqrt{1 + (3ax_e^2 + 2bx_e + c)^2} \\ (3ax_e^2 + 2bx_e + c) / \sqrt{1 + (3ax_e^2 + 2bx_e + c)^2} \end{bmatrix}.
\end{aligned}
\tag{32}
$$

B. Coordinate Conversion

For curvilinear coordinate conversion, a key component is computation of the closest point (C_o) on the CHS lane model. The closest point is numerically computed by a two-stage technique that combines quadratic minimization and Newton's method [41], which minimize the distance between the target point and a point on the CHS lane model.

The quadratic minimization makes progress toward an optimal solution, but the average rate of convergence of the quadratic minimization is slow compared to Newton's method. For this reason, quadratic minimization is suitable for rough estimation of the optimal value. When the initial estimation is sufficiently good, finding the solution by using Newton's method is fast and accurate. The reason for this advantage of Newton's method is that it uses the first and second derivative of the function. The complementary nature of these two methods prevents the divergence of the optimization and improves the rate of convergence for real-time implementation. The algorithm executes the quadratic minimization at first, in order to estimate an initial guess for Newton's method. Finally, Newton's method finds the closest point on the CHS lane model.

In order to conduct transformation between the Cartesian coordinates and the curvilinear coordinates using the CHS lane model and the closest point, the relation of Cartesian coordinates (x, y) and the curvilinear coordinates (s, q) is represented with the curvature of the CHS lane model (k_b), as follows [16]:

$$x = \left(\frac{1}{\kappa_b} - n \right) \cdot \sin(s\kappa_b) \tag{33}$$

$$y = \frac{1}{\kappa_b} - \left(\frac{1}{\kappa_b} - n \right) \cdot \cos(s\kappa_b). \tag{34}$$

The first derivative in time of the Cartesian coordinates (x, y) is induced as

$$\frac{dx}{dt} = -\frac{dn}{dt} \cdot \sin(s\kappa_b) + \frac{ds}{dt} \cdot (1 - n\kappa_b) \cdot \cos(s\kappa_b) \tag{35}$$

$$\frac{dy}{dt} = \frac{dn}{dt} \cdot \cos(s\kappa_b) + \frac{ds}{dt} \cdot (1 - n\kappa_b) \cdot \sin(s\kappa_b). \tag{36}$$

The second derivative in time of the Cartesian coordinates is also derived as

$$
\begin{aligned}
\frac{d^2x}{dt^2} = &-\left(\frac{d^2n}{dt^2} + \left(\frac{ds}{dt} \right)^2 \cdot \kappa_b \cdot (1 - n\kappa_b) \right) \cdot \sin(s\kappa_b) \\
&+ \left(\frac{d^2s}{dt^2} \cdot (1 - n\kappa_b) - 2 \cdot \frac{dn}{dt} \cdot \frac{ds}{dt} \cdot \kappa_b \right) \cdot \cos(s\kappa_b)
\end{aligned}
\tag{37}
$$

$$
\begin{aligned}
\frac{d^2y}{dt^2} = &\left(\frac{d^2n}{dt^2} + \left(\frac{ds}{dt} \right)^2 \cdot \kappa_b \cdot (1 - n\kappa_b) \right) \cdot \cos(s\kappa_b) \\
&+ \left(\frac{d^2s}{dt^2} \cdot (1 - n\kappa_b) - 2 \cdot \frac{dn}{dt} \cdot \frac{ds}{dt} \cdot \kappa_b \right) \cdot \sin(s\kappa_b).
\end{aligned}
\tag{38}
$$

In addition, the velocity information can be represented as

$$\begin{bmatrix} v_x \\ v_y \end{bmatrix} = \begin{bmatrix} \cos\psi & -\sin\psi \\ \sin\psi & \cos\psi \end{bmatrix} \begin{bmatrix} v_s \\ v_n \end{bmatrix} \tag{39}$$

where

$$\psi = \tan^{-1}\left(y'(s)/x'(s) \right). \tag{40}$$

VI. LANE ASSESSMENT

For safe maneuvering, it is important to determine the threat level of each lane, which indicates whether a lane is occupied by another vehicle or how dangerous each lane is if an ego vehicle is to change lanes. This level is simply estimated by rule-based expert systems. However, rule-based methods do not consider uncertainties in the sensor's inputs. In order to overcome this limitation, the adaptive likelihood function, which is proposed in [13], is used to estimate the lane positions of objects and risk assessment from the ego vehicle. This method divides a lane status into three conditions [Dangerous, Occupied, and Free] and represents the threat level of a lane as the probability of each lane condition. In this chapter, processes for adaptive likelihood node (ALNs) will be introduced.
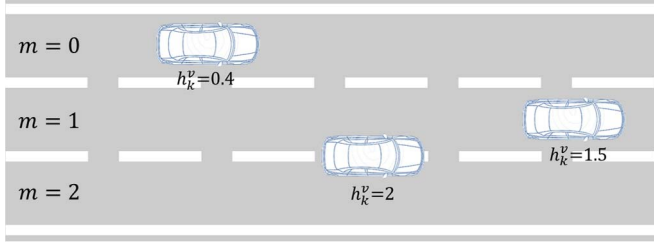
Fig. 9. NLP examples.

A. Probabilistic Lane Association

In order to determine the threat level of each lane, it is first necessary to know in which lanes the objects exist. Since the lateral–directional data (n_k^v) in curvilinear coordinates is directly related to the position in a lane, the lane association can be easily calculated. For this purpose, the normalized lateral position (NLP) is defined as

$$h_k^v = \frac{N_{\text{lane}} W_{\text{lane}} - 2n_k^v}{2W_{\text{lane}}} \qquad (41)$$

where N_{lane} and W_{lane} represent the number of lanes and the lane width, respectively. NLP provides the relative position with respect to the lanes. For example, if vehicle v is in lane 1, h_k^v is calculated between 1 and 2, as shown in Fig. 9.

In order to consider the uncertainties of objects and lanes, the likelihood function for the NLP of lane m is defined as

$$p\left(h_k^v|m\right) = \begin{cases} \exp\left(-\frac{\left(h_k^v-m\right)^2}{2w_{\text{lane}}\sigma_l^2}\right), & \text{if } h_k^v < m \\ \exp\left(-\frac{\left(h_k^v-m-1\right)^2}{2w_{\text{lane}}\sigma_l^2}\right), & \text{if } h_k^v > m+1 \\ 1, & \text{else} \end{cases} \qquad (42)$$

where σ_l is derived from a lane confidence probability provided by the camera sensor, and it takes into account the uncertainties of the sensor.

If it is assumed that the prior PDF of the lane has a uniform distribution, the probability that a vehicle is located in the lane is estimated using Bayes' theorem, as

$$P\left(m|h_k^v\right) = \frac{p\left(h_k^v|m\right)}{\sum_{i=m_{\min}}^{m_{\max}} p\left(h_k^v|i\right)}. \qquad (43)$$

B. Probabilistic Threat Assessment

The threat level of an object depends on the distance between the object and the ego vehicle, and the relative speed. For these factors, the TTC is used as a time measure. When TTC is applied for curved roads, the longitudinal distance (s_k^v) and velocity (v_k^v) in curvilinear coordinates can prevent a misunderstanding in the threat assessment because they represent the vehicle's longitudinal motion along a lane.

The TTC is defined by the relative distance and velocity in curvilinear coordinates, as

$$\text{TTC} = \frac{s_k^v - s_{\text{ego}}}{v_{\text{ego}} - v_k^v}. \qquad (44)$$

In order to represent the risk of each lane as a probability, the vehicle threat state l is defined as [Dangerous Occupied Free] $=$ $[D, O, F]$. The likelihood function for TTC under the vehicle threat state l is calculated by

$$p\left(t_{\text{inv},k}^v|l=D\right)$$

$$= \begin{cases} \exp\left(-\frac{\left(t_{\text{inv},k}^v-\bar{t}_{\text{inv}}^{\text{dan}}\right)^2}{2\sigma_t^2}\right), & \text{if } t_{\text{inv},k}^v < \bar{t}_{\text{inv}}^{\text{dan}} \\ 1, & \text{else} \end{cases} \qquad (45)$$

$$p\left(t_{\text{inv},k}^v|l=O\right)$$

$$= \begin{cases} \exp\left(-\frac{\left(t_{\text{inv},k}^v-\bar{t}_{\text{inv}}^{\text{occ}}\right)^2}{2\sigma_t^2}\right), & \text{if } t_{\text{inv},k}^v < \bar{t}_{\text{inv}}^{\text{occ}} \\ \exp\left(-\frac{\left(t_{\text{inv},k}^v-\bar{t}_{\text{inv}}^{\text{dan}}\right)^2}{2\sigma_t^2}\right), & \text{if } t_{\text{inv},k}^v > \bar{t}_{\text{inv}}^{\text{dan}} \\ 1, & \text{else} \end{cases} \qquad (46)$$

$$p\left(t_{\text{inv},k}^v|l=F\right)$$

$$= \begin{cases} \exp\left(-\frac{\left(t_{\text{inv},k}^v-\bar{t}_{\text{inv}}^{\text{occ}}\right)^2}{2\sigma_t^2}\right), & \text{if } t_{\text{inv},k}^v > \bar{t}_{\text{inv}}^{\text{occ}} \\ 1, & \text{else} \end{cases} \qquad (47)$$

where σ_t is obtained from the covariance matrices of the track-to-track fusion results. In these equations, the inverse TTC t_{inv} is used instead of TTC, in order to simplify the likelihood function $p(t_k^v|l)$. $\bar{t}_{\text{inv}}^{\text{dan}}$ and $\bar{t}_{\text{inv}}^{\text{occ}}$ are the thresholds of the dangerous and occupied states, respectively.

Under the assumption that the prior PDF of TTC follows a uniform distribution, the probability distribution of the vehicle state $P(l|t_{\text{inv},k}^v)$ is represented using Bayes' theorem, as

$$P\left(l|t_{\text{inv},k}^v\right)$$

$$= \frac{P\left(t_{\text{inv},k}^v|l\right)}{p\left(t_{\text{inv},k}^v|l=D\right) + p\left(t_{\text{inv},k}^v|l=O\right) + p\left(t_{\text{inv},k}^v|l=F\right)}. \qquad (48)$$

C. Probabilistic Lane Status

The combination of the probabilities calculated in the lane association and threat assessment determines the probability distribution of the status of lane c. The combinational relations can be derived as

$$P(L_k^c = D) = 1 - \prod_{v=1}^{v_{\max}} \left[1 - P\left(l_k^v = D\right) P\left(m_k^v = c\right)\right] \qquad (49)$$

$$P\left(L_k^c = F\right) = \prod_{v=1}^{v_{\max}} \left[1 - P\left(m_k^v = c\right)\left[1 - P\left(l_k^v = F\right)\right]\right] \qquad (50)$$

$$P\left(L_k^c = O\right) = 1 - P\left(L_k^c = D\right) - P\left(L_k^c = F\right). \qquad (51)$$

TABLE I
PARAMETERS OF TEST SCENARIO FOR COMPARISON
OF TTC PREDICTION BETWEEN CURVILINEAR
AND CARTESIAN REPRESENTATION

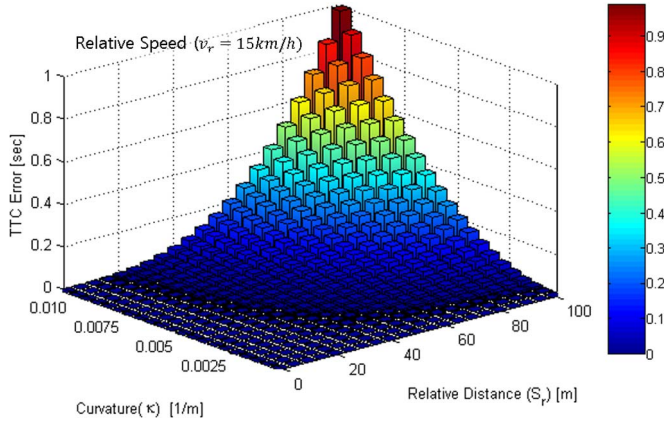| Parameter	Description	Range	Resolution	Unit
κ	Road curvatures	0 - 0.01	0.0005	1/m
s_r	Relative distance between the ego and object vehicle	0 - 100	5	m
v_r	Relative speed between the ego and object vehicle	5 - 50	5	km/h

Fig. 10. Comparison results in the prediction of TTC between curvilinear and Cartesian representations according to road curvatures (κ) and relative distance (s_r).

VII. ANALYSIS AND EXPERIMENT

A. Quantitative Evaluation of Curvilinear-Coordinate-Based and Cartesian Coordinate-Based Representations

The proposed curvilinear-coordinate-based representation provides longitudinal (s) and lateral (n) distance information along a road; consequently, the prediction of TTC is more accurate compared to the Cartesian coordinate-based representation for curved roads. Two test cases were applied to analyze the error in the prediction of the TTC between curvilinear and Cartesian representations. The test cases used an object vehicle to drive in front of the ego vehicle in the same lane. Road curvatures, relative distance, and speed are altered according to different scenarios to evaluate the representations under various conditions, as shown in Table I.

Figs. 10 and 11 depict the error in the prediction of TTC between curvilinear and Cartesian representations. The first test case in Fig. 10 assumed that the relative speed was maintained at 15 km/h, and the road curvatures and relative distance varied, as shown in Table I. In Fig. 10, the error in the prediction of TTC is very small for low-curvature roads with short relative distances; however, the error in the high-curvature and long-relative-distance condition rapidly increases up to 1 s. In the second test case, the relative distance condition was fixed at 50 m, with curvature and relative speed conditions changed, as shown in Fig. 11. Similar to the first test case, the TTC error in Fig. 11 was also increased according to the increase of curvature. However, the TTC error is reduced according
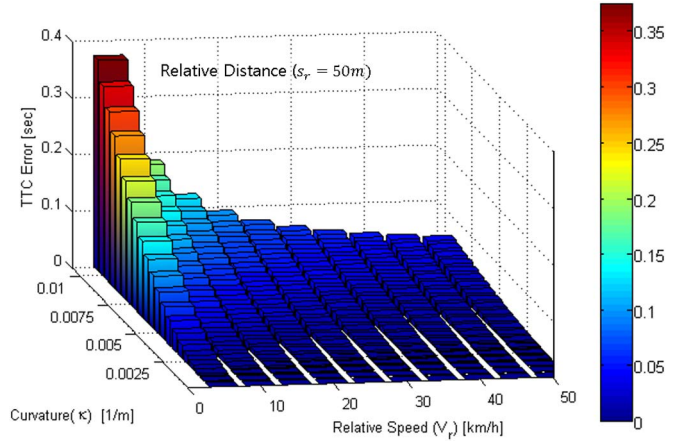

Fig. 11. Comparison results in the prediction of TTC between curvilinear and Cartesian representations according to road curvatures (κ) and relative speed (v_r).

TABLE II
SENSOR OUTPUTS

Sensor	Information
Front radar	Up to 45 objects Longitudinal position (Resolution: 0.01m) Lateral position (Resolution: 0.04m) Relative velocity (Resolution: 0.01 m/s)
Rear radar	Up to 25 objects Longitudinal and lateral position (Resolution: 0.01m) Relative velocity (Resolution: 0.01 m/s)
Camera	Right/left lane offsets (Resolution: 0.01m) Heading angle of lane (Resolution: 4e-5 rads) Curvature of lane (Resolution: 8e-7 m^{-1}) Rate of change of curvature (Resolution: 1e-6 m^{-2}) Right/left lane type (Solid/Dashed/Double/Road Edge) Right/left lane confidence (Resolution: 1.6%)

TABLE III
SENSOR SPECIFICATIONS

Sensor	Characteristics and configurations
Front radar	Type: Long range Detection range: 2m ~ 205m F.O.V: (Horizontal) ± 10deg / (Vertical) ± 2deg
Rear radar	Type: Short range Detection range: 0.4m ~ 70m F.O.V: (Horizontal) ± 75deg / (Vertical) ± 2deg
Camera	Output data: Lane parameters, lane type, lane confidence F.O.V: (Horizontal) ± 21deg

to the increase of relative speed in the case of the relative speed variation. Therefore, the TTC error is proportional to the increase of the road curvature and relative distance and inversely proportional to the increase of relative speed. The road curvature is the most important factor for TTC error in both test cases since the calculation error in the Cartesian representations increased under high-curvature road conditions. This result indicates that the curvilinear coordinates and Cartesian coordinates have a similar accuracy on straight roads; however, the Cartesian representations are inaccurate in curved roads and cannot substitute curvilinear representations.
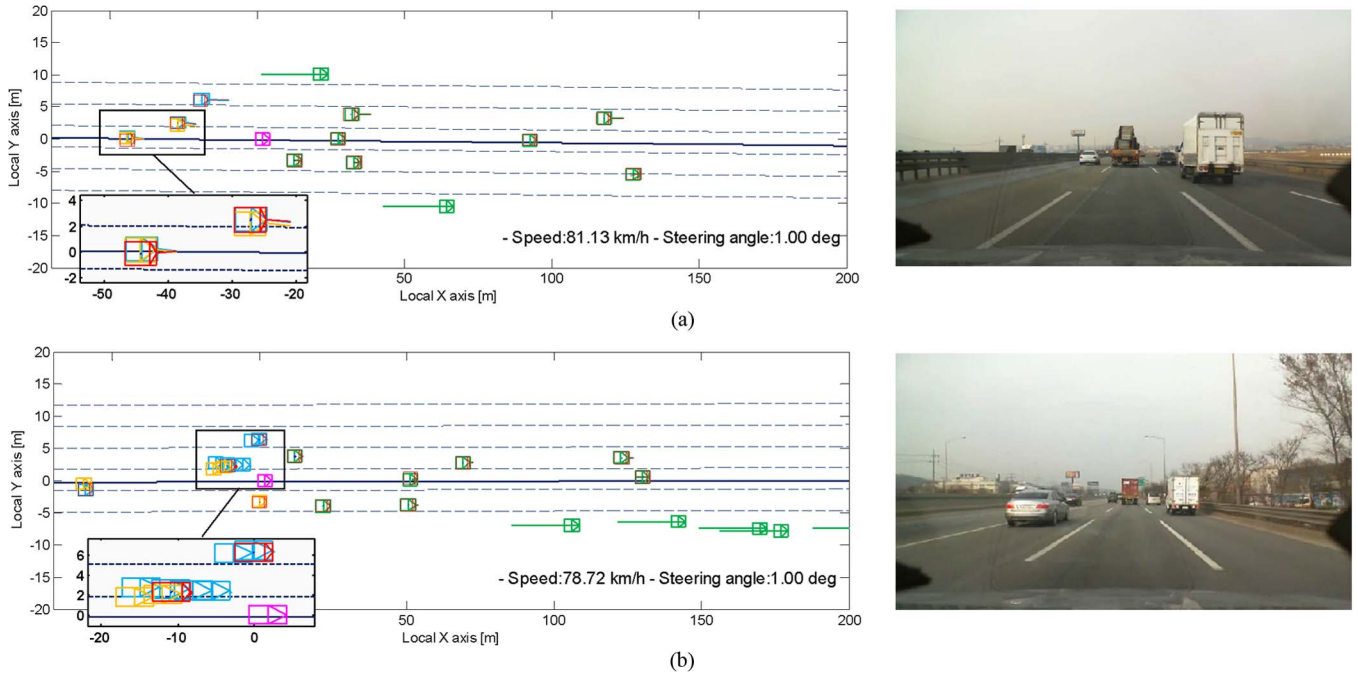
Fig. 12.   Track-to-track fusion results in highway driving cases.

B. Experimental Setup

Front radar, two rear radars, and a camera were equipped in a test vehicle to validate the proposed object and situation assessment algorithm, as shown in Fig. 3. The output and specification of the sensors are given in Tables II and III, respectively. The front radar provides object position and velocity information for object assessment. It has a detection distance range of 205 m and is installed inside the front bumper. Each rear radar also supplies object position and velocity information. It has a detection distance range of 70 m and is installed inside the edge of the rear bumper. The camera provides lane parameters, types, and confidence information. It has a horizontal field of view (FOV) of $\pm 21°$ and is mounted to the back side of the front windshield. The proposed object and situation assessment algorithm was implemented in a real-time embedded system that contained a 32-bit real-time microcontroller unit (Freescale MPC5675k). The developed embedded system has four controller area network (CAN) to communicate with each installed sensor and to obtain the motion data of the ego vehicle from the in-vehicle network. To evaluate the proposed system, the results of the assessment algorithm are compared to matched scene images from additional recorded videos during experiments.

C. Experimental Results

The experiments were carried out on the Gyeongbu expressway, which connects Seoul and Busan in South Korea. Since it consists of various curved and straight roads with a large number of moving vehicles, various test cases were performed for the evaluation of the proposed object and situation assessment algorithm. During the experiments, the ego vehicle and other moving vehicles are driven within 30 km/h and 120 km/h. The graphs and pictures shown in Figs. 12–18 illustrate the object and situation assessment results for the test cases.

In these graphs, the dashed black lines represent the detected lanes, and the black solid lines represent the generated CHS lane models. The green, blue, and yellow boxes indicate the measurements of the front, rear left, and rear right radars, respectively. The magenta box indicates the ego vehicle, and the red boxes represent the track-to-track fusion results. In these boxes, the solid lines indicate the relative velocity compared with the velocity of the ego vehicle, and the blue ellipses represent the error covariance. The pictures in each figure are snapshots of the recorded videos, which are matched with their related experiments. A related video about the test results is available at http://youtu.be/o2znweADCM4.

1) Object Assessment Results: Fig. 12 shows the track-to-track fusion results in highway driving cases. Since there are overlapped detection areas in the rear radars, as shown in Fig. 3, the track-to-track fusion was mainly performed on the rear sides. Since there are a lot of moving vehicles, the highway is suitable for evaluating the correction performance of the object assessment algorithm in duplicated measurements. As shown in Fig. 12(a) and (b), there are multiple measurements for same vehicles, but the proposed object assessment algorithm generates a fused track for each vehicle. In addition, the object assessment algorithm uses the lane model information; hence, the false-positive measurements by highway guardrail can be filtered out, and the only valid tracks are maintained.

Fig. 13 indicates the results of the track status management in an overtaking scenario. There are two vehicles that quickly become close to the ego vehicle, as shown in Fig. 13(a). When the vehicles pass by the ego vehicle, there are no measurements from the radars because they are located outside of the sensor coverage, as shown in Fig. 13(b). In spite of the lack of measurements, the tracks are maintained by the NNF with an increase in the error covariance. After moving past the ego vehicle, the vehicles are measured from the front radar, as
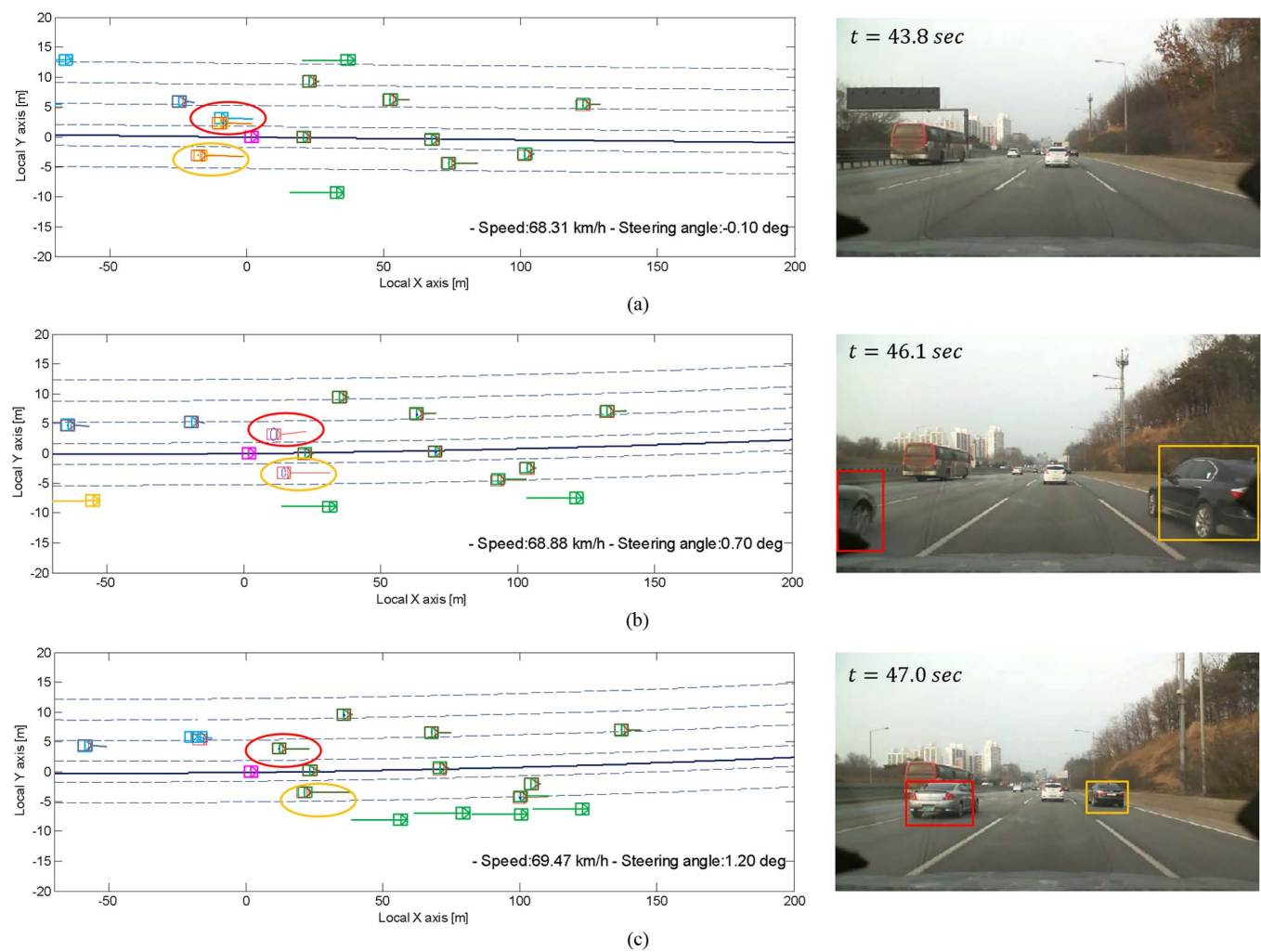
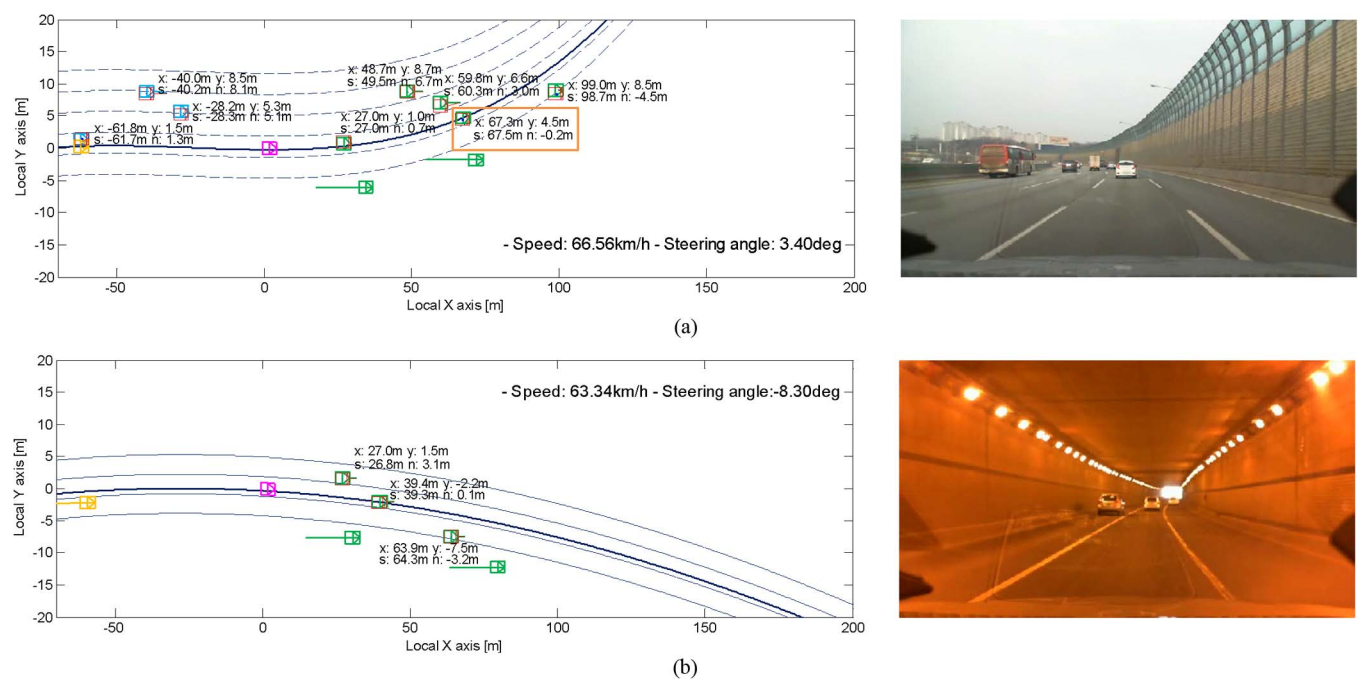Fig. 13. Track status management results in an overtaken case.

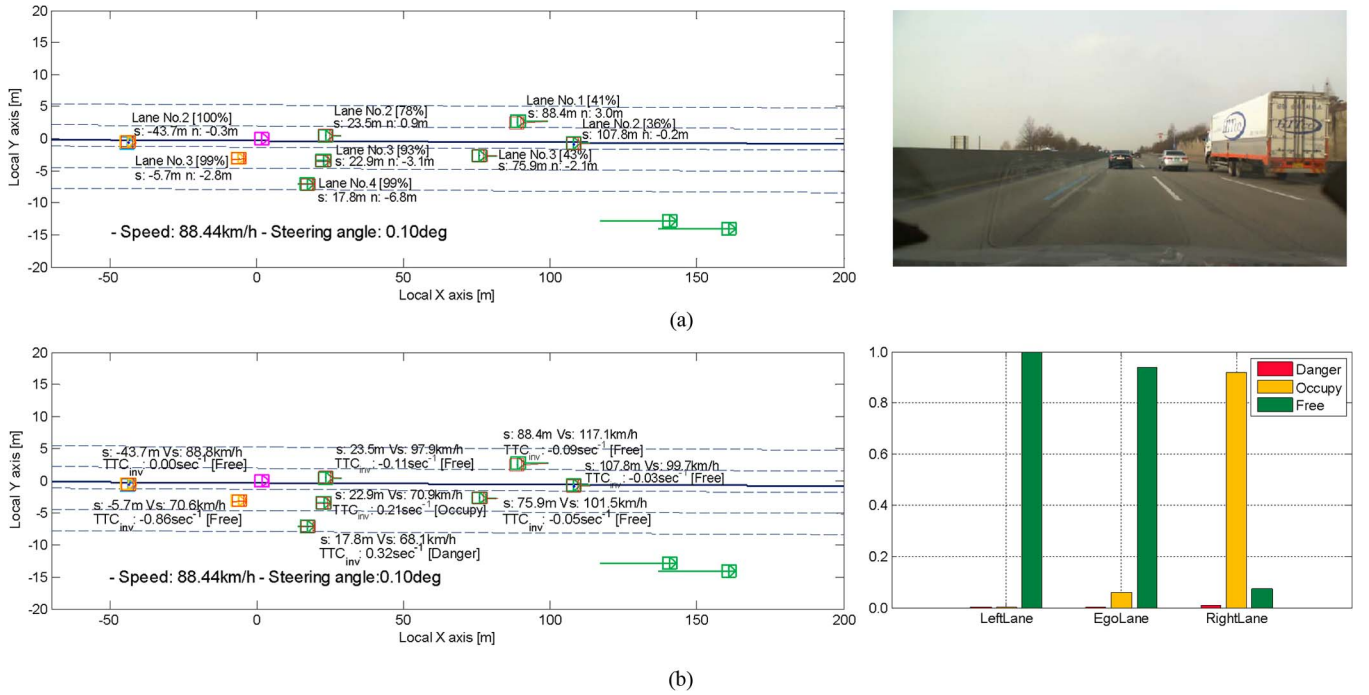Fig. 14. Object assessment results in curved road cases.

Fig. 15.   Lane association and threat assessment-based lane status in a straight road case: (a) Lane association results. (b) Threat and lane status assessment results.
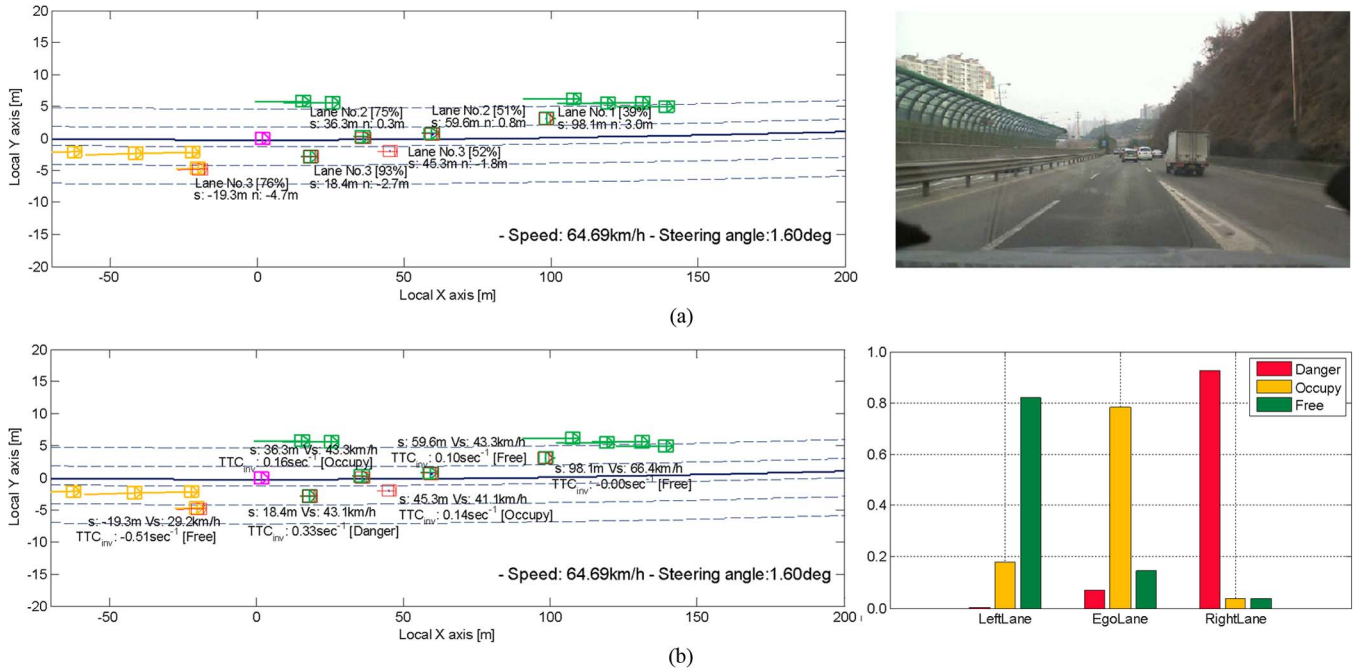

Fig. 16.   Lane association and threat assessment-based lane status in a merging road case: (a) Lane association results. (b) Threat and lane status assessment results.

shown in Fig. 13(c). As a result, the tracks are updated, and the error covariance is reduced with the measurements.

In order to evaluate the object assessment algorithms according to various curvatures, curved road experiments were also performed, as shown in Fig. 14. The graphs in Fig. 14 contain each track's position information in Cartesian coordinates (x, y) and curvilinear coordinates (s, n). In Fig. 14(a), a vehicle is located at (67.3, 4.5) on the Cartesian coordinates. Since its lateral position is bigger than the lane width, it can be misunderstood that the vehicle is located in the left lane.

In terms of the curvilinear coordinates, the vehicle is located at (67.5, −0.2); hence, it can be judged that the vehicle is in the ego lane. Therefore, the converted position information in curvilinear coordinates is useful for a situation assessment.

2) Situation Assessment Results: Figs. 15 and 16 show the lane association and threat assessment-based situation assessment results. In order to evaluate the situation assessment in acceleration and deceleration cases, the experiments are executed for a straight road and a merging road, respectively. In each figure, subfigure (a) is composed of the probabilistic results of
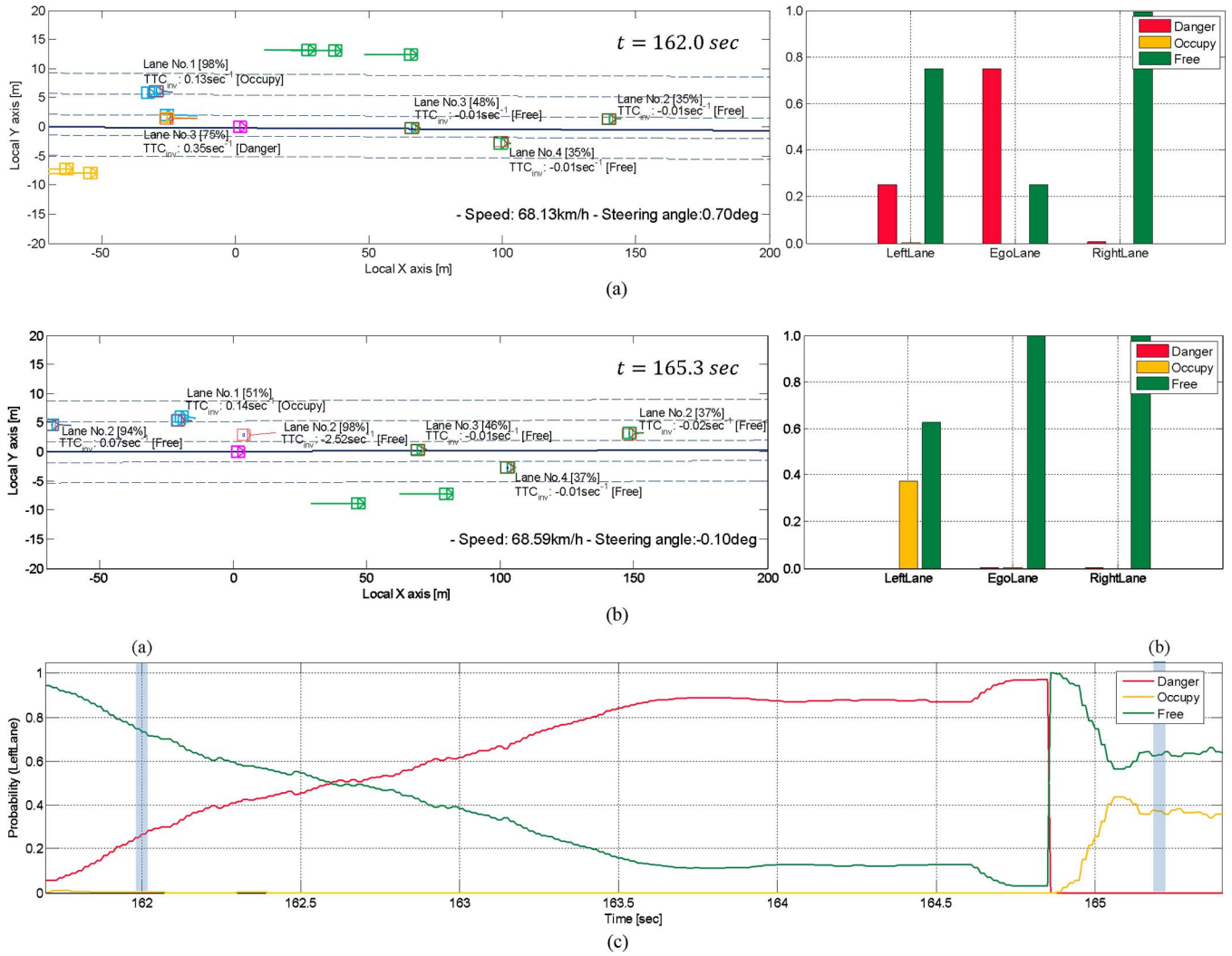
Fig. 17.   Situation assessment result in an overtaken case.

the lane association and a related snapshot, and subfigure (b) contains the probabilistic results of the threat and lane status assessment results. In subfigure (a), each track shows its position data in curvilinear coordinates and a lane number, which is the most related lane with its probabilistic value. In subfigure (b), each track indicates a value of the inverse TTC and the most related threat status. As shown in Figs. 15(a) and 16(a), some tracks that are close to the ego vehicle have high-probability lane association values with regard to the related lane. The other tracks, which are far from the ego vehicle, have relatively low values because the variance σ^2 is increased by the uncertainty changes of the tracks according to the relative distance. However, in spite of the increments of the variance σ^2, the results show that the tracks have maximum probability values in the associated lane. In terms of the threat assessment, all of the tracks are evaluated with the inverse values of TTC, as shown in Figs. 15(b) and 16(b). According to the inverse values of TTC, the probability values of each threat state are determined, and the states are indicated in Figs. 15(b) and 16(b). Based on these lane association and threat assessment results, the lane status can be determined, as shown in bar graphs in Figs. 15(b) and 16(b). In Fig. 15(b), since there is no

vehicle within 50 m in the second lane either in front or behind, the Free state has a maximum value in the left lane. Otherwise, there is a track that has the Occupied state in the third lane; hence, the Occupied state has a maximum value in the right lane. In Fig. 16(b), the Dangerous state is dominant in the right lane by the similar principle.

In order to evaluate the results of the lane status assessment according to time change, two different experiments are performed, as shown in Figs. 17 and 18. In Fig. 17(a), there is a fast moving vehicle behind the ego vehicle. Since the fast vehicle overtakes the ego vehicle through the left lane, the dominant state of the left lane is changed from Free to Dangerous, as shown in Fig. 17(c). After finishing the overtaking, another vehicle in the Occupied state changes lanes to the second lane, as shown in Fig. 17(b). As a result, the probability of the Occupied state in the left lane is gradually increased, as shown in Fig. 17(c). In Fig. 18(a) and (b), a vehicle in the right lane slows down as it enters the curved road. Due to deceleration, the state of the related track is changed from Occupied to Dangerous. As a result, the dominant state of the right lane is also converted from Occupied to Dangerous. All of these results show that the proposed algorithm continuously evaluates the lane status.
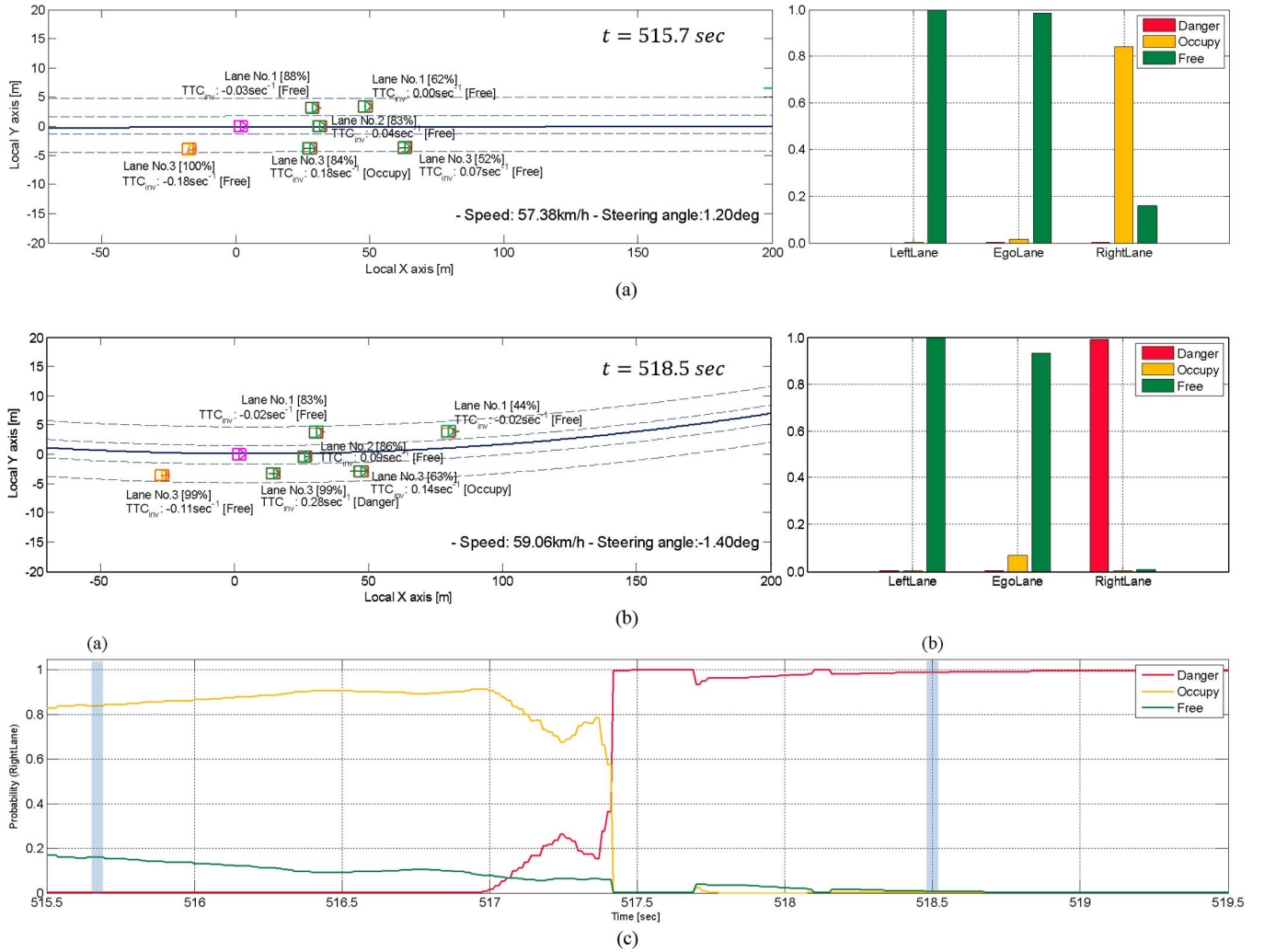
Fig. 18. Situation assessment result in a curved road case.

3) Comparison Study for Performance Evaluation of Curvilinear-Coordinate-Based Assessment Algorithm: In order to evaluate the effect of the curvilinear coordinate conversion, two conventional lane models (the Cartesian coordinate-based cubic polynomial model and the circle model) were compared with the proposed algorithm, as shown in Fig. 19. The cubic polynomial model is a commonly used method to represent lanes with four parameters. The camera that is used in these experiments also provides lane information using the cubic polynomial model. The circle model was applied in [19] as a stable method for representing the lanes.

a) Comparison of lane association with different lane models: The lane association was performed using three tracks in a curved road to understand the effect of the lane model, as shown in Fig. 19(a). The same radar and camera data in this situation were applied for the three different lane models. Each result shows the lateral offset of each track and the number of iterative computations to satisfy the desired tolerances to numerically calculate the offset. As shown in Fig. 19(b) and (d), the lateral offsets are almost the same in both the Cartesian coordinate-based cubic polynomial model and the curvilinear-coordinate-based CHS model. However, more iterations are required in the cubic polynomial case because it is sensitive to

changes in the curvature of curved roads. Otherwise, the circle model requires less iteration than other models because it can easily derive the lateral offsets from the radius and position information. However, the circle model's results reveal some errors in representing the road geometry because there is no curvature change according to the longitudinal distance, as shown in Fig. 19(c). As a result, the lateral position of each track in the lanes can be misunderstood, which reduces the accuracy of the lane association.

Table IV shows the analysis results for the accuracy of the lane association according to the lane models. In the analysis, the success rate was obtained by manually comparing the lane association results and lane of tracks from the video data. Table IV shows that the circle model shows relatively poor performance compared to other models because the lane association results have big errors when the location of tracks is far from the lane of the ego vehicle. The cubic polynomial model shows a high success rate of over 90% (the fail results mainly occurred in curved road cases); however, the curvilinear-coordinate-based CHS has a high success rate in curved roads and straight roads. The success rate of CHS will increase if the track and lane information from sensors is more accurate and stable because the lane association of the proposed
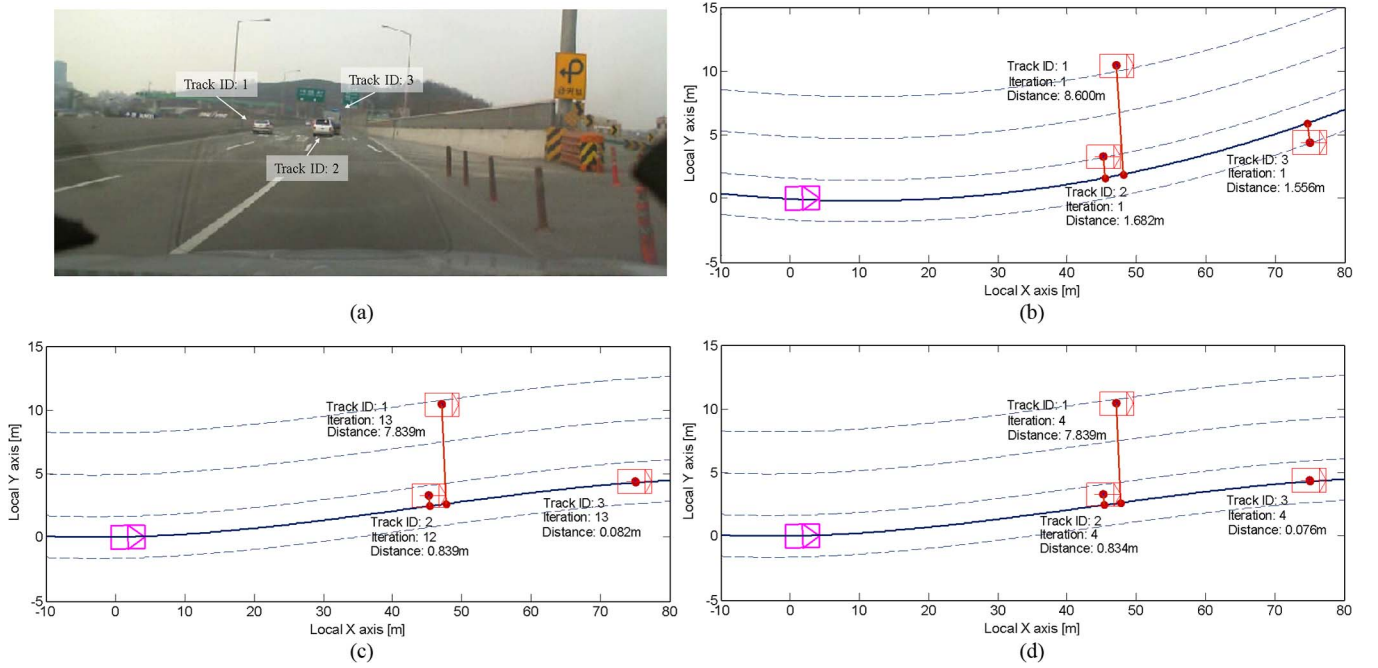
Fig. 19. Comparison result of lane association with different lane models. (a) Reference scene. (b) Cartesian coordinate-based circle model. (c) Cartesian coordinate-based cubic polynomial model. (d) Curvilinear-coordinate-based CHS model.

TABLE IV
PERFORMANCE ANALYSIS ABOUT LANE ASSOCIATION
WITH DIFFERENT LANE MODELS

Lane Model	Properties	Success rate of Lane Association
Circle	Highway Sequence 1 (7 min 30 sec)	32.22 %
	Highway Sequence 2 (8 min 45 sec)	28.72 %
Cubic Polynomial	Highway Sequence 1 (7 min 30 sec)	90.45 %
	Highway Sequence 2 (8 min 45 sec)	91.87 %
Cubic Hermite Spline	Highway Sequence 1 (7 min 30 sec)	94.71 %
	Highway Sequence 2 (8 min 45 sec)	95.82 %

Fig. 20. Number of iteration to calculate lateral offsets according to rate of change of curvature for each lane model.

method shows excellent performance without regard to road shapes.

b) Analysis of Required Iterative Computation Depending on Rate of Change of Curvature: Fig. 20 shows the total number of iterative computations required to calculate the lateral position of about 20 tracks in each lane model. Since the Cartesian coordinate-based cubic polynomial model has a convergence speed problem caused by sensitivity to the rapid change of the curvature, the number of iterations of the cubic polynomial model shows an increasing tendency according to the rate of change of the curvature, as shown in Fig. 20. This result implies that the maximum number of tracks or the maximum error tolerance should be reduced for real-time computation. Otherwise, since the CHS model is converted to curvilinear coordinates, the effect of change of the curvature is relatively low, and the maximum number of iterations is much smaller than it is for the cubic polynomial. Therefore, the curvilinear-coordinate-based CHS model is more suitable for real-time applications.
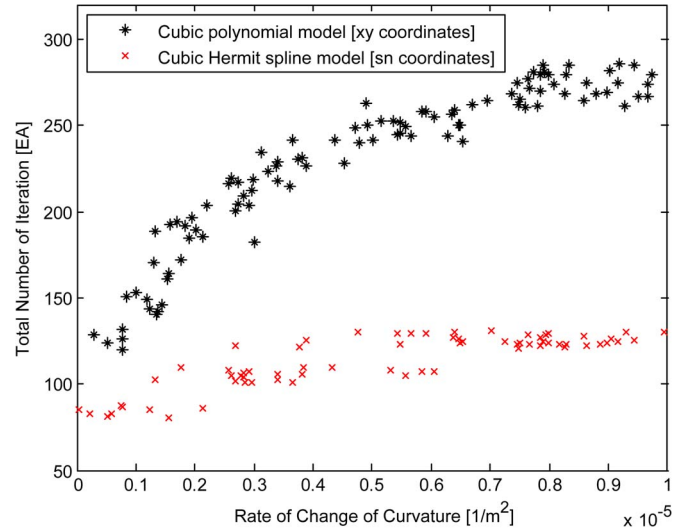
A comparison study shows that the curvilinear coordinate conversion can reduce the number of iterative computations needed to calculate the lateral offset for lane association. This advantage can reduce the computation time for real-time automotive applications and can improve the accuracy of the object and situation assessment.

VIII. CONCLUSION

In this paper, we have described the development of an object and situation assessment system that is based on track-to-track fusion and probabilistic lane assessment for use in highly automated driving applications. The developed object and situation assessment system integrates object information

from the radars and lane information from a camera. In order to improve the performance of the assessment system for various road geometries, the integration process is composed of three steps. The first step is the track-to-track fusion process that merges duplicate measurements from the radars. In the fusion step, the NNF is applied to synchronize the radar measurements and to provide correlation information. Based on the tracks, which are updated by the NNF, the CCM fuses duplicate tracks using the error covariance. The second step is the curvilinear coordinate conversion, which converts the position and velocity information of each track into curvilinear coordinates. Curvilinear coordinates are derived from the lane information of a camera with a CHS lane model. To find position information in the lane model, the numerical search technique, which combines quadratic minimization and Newton's method, is applied. The third step is the lane assessment, which determines the threat levels of the surrounding lanes in a stochastic manner. In order to evaluate the lane association of each track, an ALN is applied with an NLP. For threat assessment of each track, TTC is used as a collision evaluation index. Finally, the probability distribution of the lane status is determined from the combination of the probabilities calculated in the lane association and threat assessment.

In order to validate the proposed object and situation assessment algorithm, it was implemented in a real-time embedded system, and various experiments were performed on the Gyeongbu expressway in South Korea. The experimental results showed that the assessment performance was sufficiently reliable under various road curvatures and false-positive sensor measurements. In particular, the proposed curvilinear-coordinate-based CHS model provides excellent performance of lane association, in respect of accuracy and computational efficiency. Compared to the Cartesian coordinate-based circle model, which has meter-level error of lane association, the CHS model can provide more accurate entity position on lanes within centimeter-level errors. In respect of robustness in real-time computation, the Cartesian coordinate-based cubic polynomial model showed increased iteration counts to compute lane association according to the rate of change of the curvature; otherwise, the CHS model showed consistent computation results. Since the reliable computation is an important factor for the robust real-time operation, the CHS model is more suitable for real-time applications. However, since the proposed algorithm is based on lane information from the camera, the performance is limited based on the quality of the lane information. If the accuracy of detected lane position is poor by road conditions or illumination, the performance of the proposed object and situation assessment is seriously degraded. In order to overcome this limitation, the authors plan to extend the object and situation assessment algorithm to consider other information, such as a centimeter-level high-quality navigation map [42]–[44]. The integration of map information will improve object and situation assessment under various driving conditions. In addition, each algorithm will be improved through artificial intelligent techniques to interpret complex and various situations that can apply the proposed curvilinear-coordinate-based approach under more complicated driving situations such as urban roads that include motorbikes and pedestrians.

REFERENCES

[1] T. Robinson, E. Chan, and E. Coelingh, "Operating platoons on public motorways: An introduction to the SARTRE platooning programme," in *Proc. 17th World Congr. Intell. Transp. Syst.*, 2010, pp. 1–11.

[2] C. Bergenhem, Q. Huang, A. Benmimoun, and T. Robinson, "Challenges of platooning on public motorways," in *Proc. 17th World Congr. Intell. Transp. Syst.*, 2010, pp. 1–12.

[3] F. Flemisch et al., "Towards highly automated driving: Intermediate report on the HAVEit-Joint system," in *Proc. Eur. Transp. Res. Arena Conf.*, 2010, pp. 7–10.

[4] R. Hoeger et al., "Highly automated vehicles for intelligent transport: Have-it approach," in *Proc. 15th World Congr. ITS*, 2008, pp. 1–10.

[5] C. Baker and J. Dolan, "Street smarts for boss," *IEEE Robot. Autom. Mag.*, vol. 16, no. 1, pp. 78–87, Mar. 2009.

[6] C. Urmson et al., "Autonomous driving in urban environments: Boss and the Urban Challenge," *J. Field Robot.*, vol. 25, no. 8, pp. 425–466, Aug. 2008.

[7] R. Kianfar et al., "Design and experimental validation of a cooperative driving system in the Grand Cooperative Driving Challenge," *IEEE Trans. Intell. Transp. Syst.*, vol. 13, no. 3, pp. 994–1007, Sep. 2012.

[8] A. Geiger et al., "Team AnnieWAY's entry to the 2011 Grand Cooperative Driving Challenge," *IEEE Trans. Intell. Transp. Syst.*, vol. 13, no. 3, pp. 1008–1017, Sep. 2012.

[9] J. Ibañez-Guzmán, C. Laugier, J.-D. Yoder, and S. Thrun, "Autonomous driving: Context and state-of-the-art," in *Handbook of Intelligent Vehicles*, A. Eskandarian, Ed. London, U.K.: Springer-Verlag, 2012, pp. 1271–1310.

[10] M. E. Liggins, D. L. Hall, and J. Llinas, *Handbook of Multisensor Data Fusion: Theory and Practice*, vol. 22. Boca Raton, FL, USA: CRC Press, 2008.

[11] F. E. White, Data Fusion Lexicon, DTIC Document1991.

[12] A. N. Steinberg, C. L. Bowman, and F. E. White, "Revisions to the JDL data fusion model," in *Proc. AeroSense*, 1999, pp. 430–441.

[13] R. Schubert and G. Wanielik, "A unified Bayesian approach for object and situation assessment," *IEEE Intell. Transp. Syst. Mag.*, vol. 3, no. 2, pp. 6–19, 2011.

[14] C. Laugier et al., "Probabilistic analysis of dynamic scenes and collision risks assessment to improve driving safety," *IEEE Intell. Transp. Syst. Mag.*, vol. 3, no. 4, pp. 4–19, 2011.

[15] K. Chu, M. Lee, and M. Sunwoo, "Local path planning for off-road autonomous driving with avoidance of static obstacles," *IEEE Trans. Intell. Transp. Syst.*, vol. 13, no. 4, pp. 1599–1616, Dec. 2012.

[16] T. Barfoot and C. M. Clark, "Motion planning for formations of mobile robots," *Robot. Auton. Syst.*, vol. 46, no. 2, pp. 65–78, Feb. 2004.

[17] M. Werling, J. Ziegler, S. Kammel, and S. Thrun, "Optimal trajectory generation for dynamic street scenarios in a Frenet frame," in *Proc. IEEE ICRA*, 2010, pp. 987–993.

[18] B. R. Kusse and E. A. Westwig, *Mathematical Physics: Applied Mathematics for Scientists and Engineers*, 2nd ed. Hoboken, NJ, USA: Wiley, 2007.

[19] R. Schubert, K. Schulze, and G. Wanielik, "Situation assessment for automatic lane-change maneuvers," *IEEE Tans. Intell. Transp. Syst.*, vol. 11, no. 3, pp. 607–616, Sep. 2010.

[20] S. Yue, D. Yuhan, and S. Xiuming, "Asynchronous track fusion in a multi-scale sensor environment," in *Proc. Joint Conf. 10th Asia-Pacific Conf. Commun. 5th Int. Symp. Multi-Dimensional Mobile Commun. Proc.*, 2004, vol. 1, pp. 323–327.

[21] Z. Liu, M. Wang, and J. Huang, "An evaluation of several fusion algorithms for multi-sensor tracking system," *J. Inf. Comput. Sci.*, vol. 7, no. 10, pp. 2101–2109, 2010.

[22] K. C. Chang, R. K. Saha, and Y. Bar-Shalom, "On optimal track-to-track fusion," *IEEE Trans. Aerosp. Electron. Syst.*, vol. 33, no. 4, pp. 1271–1276, Oct. 1997.

[23] Y. Bar-Shalom and X.-R. Li, *Multitarget-Multisensor Tracking: Principles and Techniques*. Storrs, CT, USA: Univ. of Connecticut Press, 1995.

[24] S. Matzka and R. Altendorfer, "A comparison of track-to-track fusion algorithms for automotive sensor fusion," in *Proc. IEEE Int. Conf. MFI*, 2008, pp. 189–194.

[25] Y. Bar-Shalom, "On the track-to-track correlation problem," *IEEE Trans. Autom. Control*, vol. 26, no. 2, pp. 571–572, Apr. 1981.

[26] K. U. Jeffrey and J. Simon, "General decentralized data fusion with covariance intersection," in *Handbook of Multisensor Data Fusion*. Boca Raton, FL, USA: CRC Press, 2008, pp. 319–343.

[27] J. K. Uhlmann, "Covariance consistency methods for fault-tolerant distributed data fusion," *Inf. Fusion*, vol. 4, no. 3, pp. 201–215, Sep. 2008.

[28] C. Chee-Yee, K.-C. Chang, and S. Mori, "Distributed tracking in distributed sensor networks," in *Proc. Am. Control Conf.*, 1986, pp. 1863–1868.

[29] J. Hillenbrand, A. M. Spieker, and K. Kroschel, "A multilevel collision mitigation approach—Its situation assessment, decision making, performance tradeoffs," *IEEE Trans. Intell. Transp. Syst.*, vol. 7, no. 4, pp. 528–540, Dec. 2006.

[30] A. Polychronopoulos *et al.*, "Dynamic situation and threat assessment for collision warning systems: The EUCLIDE approach," in *Proc. IEEE Intell. Veh. Symp.*, 2004, pp. 636–641.

[31] J. Hillenbrand, A. Spieker, and K. Kroschel, "Efficient decision making for a multi-level collision mitigation system," in *Proc. IEEE Intell. Veh. Symp.*, 2006, pp. 460–465.

[32] A. Eidehall and L. Petersson, "Statistical threat assessment for general road scenes using Monte Carlo sampling," *Intell. Transp. Syst.*, vol. 9, no. 1, pp. 137–147, Mar. 2008.

[33] J. Schneider, A. Wilde, and K. Naab, "Probabilistic approach for modeling and identifying driving situations," in *Proc. IEEE Intell. Veh. Symp.*, 2008, pp. 343–348.

[34] M. Althoff, O. Stursberg, and M. Buss, "Model-based probabilistic collision detection in autonomous driving," *IEEE Trans. Intell. Transp. Syst.*, vol. 10, no. 2, pp. 299–310, Jun. 2009.

[35] A. Borkar, M. Hayes, and M. T. Smith, "Robust lane detection and tracking with RANSAC and Kalman filter," in *Proc. 16th IEEE ICIP*, 2009, pp. 3261–3264.

[36] C. Hsu-Yung, J. Bor-Shenn, T. Pei-Ting, and F. Kuo-Chin, "Lane detection with moving vehicles in the traffic scenes," *IEEE Trans. Intell. Transp. Syst.*, vol. 7, no. 4, pp. 571–582, Dec. 2006.

[37] D. Zhang, K. Li, and J. Wang, "Radar-based target identification and tracking on a curved road," *Proc. Inst. Mech. Eng. Part D, J. Automobile Eng.*, vol. 226, no. 1, pp. 39–47, Jan. 1, 2012.

[38] Y. Yamada, S. Tokoro, and Y. Fujita, "Development of a 60 GHz radar for rear-end collision avoidance," in *Proc. Intell. Veh. Symp.*, 1994, pp. 207–212.

[39] X. Rong Li and Y. Bar-Shalom, "Tracking in clutter with nearest neighbor filters: Analysis and performance," *IEEE Trans. Aerosp. Electron. Syst.*, vol. 32, no. 3, pp. 995–1010, Jul. 1996.

[40] T. L. Song, D. Gwan Lee, and J. Ryu, "A probabilistic nearest neighbor filter algorithm for tracking in a clutter environment," *Signal Process.*, vol. 85, no. 10, pp. 2044–2053, Oct. 2005.

[41] H. Wang, J. Kearney, and K. Atkinson, "Robust and efficient computation of the closest point on a spline curve," in *Proc. 5th Int. Conf. Curves Surfaces*, 2002, pp. 397–406.

[42] S. Durekovic and N. Smith, "Architectures of map-supported ADAS," in *Proc. IEEE IV Symp.*, 2011, pp. 207–211.

[43] J. Craig, "Map Data for ADAS," in *Handbook of Intelligent Vehicles*. New York, NY, USA: Springer-Verlag, 2012, pp. 881–892.

[44] P. Bender, J. Ziegler, and C. Stiller, "Lanelets: Efficient map representation for autonomous driving," in *Proc. IEEE Intell. Veh. Symp.*, 2014, pp. 420–425.

Junsoo Kim (S'11) received the B.S. degree in mechanical engineering in 2008 from Hanyang University, Seoul, Korea, where he is currently working toward the Ph.D. degree with the Automotive Control and Electronics Laboratory.

His main fields of interest are in vehicle control, decision theories, path-planning algorithms, and real-time systems. His research activities include behavior reasoning and trajectory planning of highly automated vehicles. He has also worked on model-based embedded software development for automotive control systems.

Kichun Jo (S'10–M'14) received the B.S. degree in mechanical engineering and the Ph.D. degree in automotive engineering from Hanyang University, Seoul, Korea, in 2008 and 2014, respectively.

He is currently with the Automotive Control and Electronics Laboratory, Department of Automotive Engineering, Hanyang University. His main research interests are in autonomous driving systems, information fusion theories, distributed control systems, real-time embedded systems, and in-vehicle networks. His research activities include system design and implementation of autonomous cars.

Wontaek Lim (S'14) received the B.S. degree in mechanical engineering in 2013 from Hanyang University, Seoul, Korea, where he is currently working toward the M.S. degree with the Automotive Control and Electronics Laboratory.

His research interests include path planning, vehicle control, real-time systems, and intelligent transportation systems. His research activities include path-planning algorithms and system integration for autonomous vehicles.

Minchul Lee (S'14) received the B.S. degree in mechanical engineering in 2013 from Hanyang University, Seoul, Korea, where he is currently working toward the M.S. degree with the Automotive Control and Electronics Laboratory.

His main research interests are in precise positioning and localization, information fusion theories, and real-time systems for autonomous car. His research activities include vehicle localization for autonomous cars and model-based embedded software development for automotive control systems.

Myoungho Sunwoo (M'81) received the B.S. degree in electrical engineering from Hanyang University, Seoul, Korea, in 1979; the M.S. degree in electrical engineering from University of Texas at Austin, Austin, TX, USA, in 1983; and the Ph.D. degree in system engineering from Oakland University, Rochester, MI, USA, in 1990.

In 1985 he joined General Motors Research (GMR) Laboratories, Warren, MI, USA. He has worked in the area of automotive electronics and control for 28 years. During his nine-year tenure at GMR, he worked on the design and development of various electronic control systems for powertrains and chassis. Since 1993 he has led research activities as a Professor with the Department of Automotive Engineering, Hanyang University (one of the largest engineering schools in Korea), Seoul, Korea. His work has focused on automotive electronics and controls (such as modeling and control of internal combustion engines, design of automotive distributed real-time control systems, intelligent autonomous vehicles, and automotive education programs). During his professional career, he has published 65 papers in international journals and presented 68 international conference papers. He holds 25 patents. In addition, he successfully accomplished more than 50 research projects with the Korean government and automotive companies such as Hyundai, Kia, Mando, Hyundai MOBIS, and Freescale. He has continuously consulted for the Korean government and the automotive industry.

Dr. Sunwoo was the Chairman of the Steering Committee for the Green Car Strategy Forum of the Ministry of the Knowledge Economy and is also a Senior Member of the National Academy of Engineering of Korea. In recognition of his distinguished achievements, he has received notable awards, such as the Grand Award of Academic-Industrial Cooperation from the Korean Academic-Industrial Foundation, the Best Scientist/Engineer Award of the Month from the Korean Ministry of Science and Technology, and the Award for Technology Innovation from the Prime Minister of Korea. His laboratory, i.e., Automotive Control and Electronics Laboratory, has been selected as a National Research Laboratory by the Korean government for its outstanding research accomplishments. His autonomous vehicle "A1" won the First and Second National Autonomous Vehicle Competition organized by Hyundai Motor Company hosted in Korea, in November 2010 and September 2012, respectively.